Ab-initio investigation of $A\mathrm{GeO_3}$ (A = Ca, Sr) compounds via Tran–Blaha-modified Becke–Johnson exchange potential*

Rasul Bakhsh Behram[1,2], M A Iqbal[3], Muhammad Rashid[4,†], M Atif Sattar[5], Asif Mahmood[6], and Shahid M Ramay[7,‡]

[1] *Physics Department, University of the Punjab, Quaid-e-Azam Campus, Lahore* 54590, *Pakistan*
[2] *Allama Iqbal Open University, Regional Campus, Lahore* 54590, *Pakistan*
[3] *Department of Physics, School of Science, University of Management and Technology, Lahore* 54590, *Pakistan*
[4] *Department of Physics, COMSATS Institute of Information Technology, Islamabad* 44000, *Pakistan*
[5] *Department of Physics Simulation Lab, The Islamia University of Bahawalpur, Bahawalpur* 63100, *Pakistan*
[6] *Chemical Engineering Department, College of Engineering, King Saud University, Riyadh* 11451, *Saudi Arabia*
[7] *Physics and Astronomy Department, College of Science, King Saud University, Riyadh* 11451, *Saudi Arabia*

(Received 30 May 2017; revised manuscript received 31 July 2017; published online 29 September 2017)

We employ *ab-initio* calculations to analyze the mechanical, electronic, optical and also thermoelectric properties associated with $A\mathrm{GeO_3}$ (A = Ca, Sr) compounds. The full-potential linearized augmented plane wave (FP-LAPW) technique in the generalized gradient approximation (GGA-PBEsol) and the lately designed Tran–Blaha-modified Becke–Johnson exchange potential are utilized to examine the mechanical and optoelectronic properties respectively. To explore the thermoelectric quality, we use the semi-classical Boltzmann transport theory. The particular structural stabilities regarding $A\mathrm{GeO_3}$ (A = Ca, Sr) materials are validated simply by computations from the elastic constants. The energy band structural framework and the density of states are displayed to indicate indirect bandgap under ambient conditions. The particular computed optical attributes that reveal prospective optoelectronic applications are usually elucidated simply by studying $\varepsilon_1(0)$ and also E_g, which can be connected by means of Penn's design. The optical details uncover the actual suitability to power ranging products. Finally, the BoltzTraP code is executed to analyze the actual thermoelectric properties, which usually presents that the increase of internal temperatures can enhance the electric conductivity, thermal conductivity and also the power factor, whilst Seebeck coefficient decreases. Therefore, the studied materials will also be ideal for thermoelectric products to understand helpful option for alternative energy resources.

Keywords: semiconductors, elastic properties, optical properties, thermal properties

PACS: 61.82.Fk, 87.19.rd, 91.60.Mk **DOI:** 10.1088/1674-1056/26/11/116103

1. Introduction

Since the essential multifunctional compounds, the perovskite-type oxide materials ($AB\mathrm{O_3}$) have been among the concentrates within material researches and geological science, because of their significant fascinating physical and chemical substance properties, such as superconductivities, surface properties, optical catalytic actions, uncommon permanent magnetic, pyroelectric, and ferroelectric properties.[1–5] Among such materials, the perovskites $AB\mathrm{O_3}$ (A = Mg, Ca, Sr, Cd; B=Sn, Si, Ge, Ti) manifest specific curiosities in which earth scientists are interested, and they are thought to be the most crucial components within the Earth'smantle and also have already been intensively analyzed.[6–10] Among these, the $\mathrm{CaGeO_3}$ and $\mathrm{SrGeO_3}$ materials have additionally drawn lots of interest because they are superbcrystal analogues of nutrient perovskite within the Earth's mantle. Both mineral perovskites, using the perovskite framework (that is steady at pressures more than 6 GPa) tend to be $\mathrm{GdFeO_3}$-type perovskites.[11] With temperature increasing, $\mathrm{CaTiO_3}$ experiences change under ambient conditions from orthorhombic (*Pbnm*) construction to a tetragonal ($I4/mcm$) poly-morph at temperatures between 1373 K and 1423 K, accompanied by a variation of the cubic (Pm-3m) aristotype at 1523 K.[12] High-temperature x-ray powder diffraction experimentations by Liu *et al.*[13] proposed that $\mathrm{CaGeO_3}$ perovskite goes through the phase changeover from 520 K to some structures tentatively discovered as having (*Cmcm*) symmetry, even though using high-temperature Raman scattering the obtained results demonstrated absolutely no evidence of whether the phase changeover or even soft-mode behavior takes place at temperatures between room temperature and 923 K.[14]

Currently, $\mathrm{CaGeO_3}$ and $\mathrm{SrGeO_3}$ continue to be extensively investigated experimentally[15–19] and also theoretically.[20,21] Most of studies are related to phase transfers, for example, Andrault and Poirier[15] identified that the orthorhombic structure of $\mathrm{CaGeO_3}$ is converted into the tetragonal structure at approximately 12 GPa, through using the extended x-ray absorption fine structure (EXAFS). Nonetheless, Lu and Hofmeister[16] suggested that the phase transition from

*Project supported by the Deanship of Scientific Research at King Saud University, Saudi Arabia (Grant No. RGP-VPP-311).
†Corresponding author. E-mail: muhammad.rashid@comsats.edu.pk
‡Corresponding author. E-mail: rapakistana@yahoo.com
© 2017 Chinese Physical Society and IOP Publishing Ltd

the orthorhombic to the tetragonal phases does not happen until 24.4 GPa in the far-infrared experiment. Lately, Liu and Li[17] noticed that neither discontinuities nor even elasticity conditioning for the bulk or even shear modulus exists until pressure reaches as high as 10 GPa, indicated by the results measured through using the ultrasonic interferometer.

On the other hand, Grzechnik *et al.*[18] investigated the particular stability and dielectric attribute of $SrGeO_3$ perovskite and also reported that this material is stable at above 6 GPa and 1273 K. The particular creation and phase transformation of $SrGeO_3$ happen simply by solid-state effect of $SrCO_3$ and GeO_2 coming from amorphous compound formed by the simultaneous hydrolyses of Sr and Ge isopropoxides which were noted by Yamaguchi *et al.*[19] Fang and Ahuja[20] theoretically identified that the lattice distortion with the orthorhombic $CaGeO_3$ improves with strain improving, indicated by the results from the projector-augmented wave (PAW) approach. Henriques *et al.*[21] studied the structural, electronic and also optical attributes by the local density approximation (LDA) and the generalized gradient approximation (GGA).

In any case, to the best of our knowledge, there are no hypothetical references detailing the physical properties of the cubic $CaGeO_3$ and $SrGeO_3$. The investigations of the materials exhibiting simple (e.g., cubic) crystal structures, are desired by the scientific community as they offer a better understanding of the demonstrated physical properties, and it enables one to design electronic devices with optimal performance. As is well known, the applied pressure and the temperatures can induce novel crystalline phases. Similarly, novel material phases are possible to be stabilized by using non-equilibrium growth conditions in molecular beam epitaxy (MBE). Therefore, the primary goal of this paper is to theoretically explore the mechanical, electronic, optical and thermoelectric properties associated with cubic $CaGeO_3$ and $SrGeO_3$ perovskite materials, since the theoretical research is very essential to applying all advantages of these properties to numerous practical applications. In addition, we examine the thermoelectric properties comprehensively, because the common minerals are accounted for to be an appropriate material for accomplishing high thermoelectric (TE) productivity.[22,23] The particular $CaGeO_3$ and $SrGeO_3$ might be missionary nutrients considered as a material pertaining to utilization in purposes of energy farming and also in the energy conversion process. Depending on this, the TE properties of the cubic $CaGeO_3$ and $SrGeO_3$ are studied through the use of Boltzmann transportation equation.[24]

2. Calculation method

The theoretical techniques and inexpensively obtainable computational methods have received much attention from the material researchers in order to calculate the exact material behavior, which in any other case is generally probable by high-priced experimental techniques. In this way, hypothetical strategies encourage material researchers to consider system layout architectures by computing the expected material properties before making use of experimentations. The current research entails density functional theory (DFT) dependent computations, through Wein2K code by using full potential-linearized augmented plane wave plus local orbital (FP-LAPW + lo) method.[25] The studied structures are optimized by applying the Perdew–Burke–Ernzerhof approximation (PBEsol)[26] and the ground state constraints have been evaluated through the Murnaghan's equations.[27] No doubt, the PBEsol gives better results than LDA, GGA, and PBE-GGA approximations but underestimates the band gap. Blaha *et al.*'s[25] modified potential defined by Becke and Johnson[27] is used to improve the electronic structures for accurate calculation of band gap. Consequently, we now use the lately developed modified Becke Johnson (mBJ) functional that is well known for figuring the energy band gap that is coherent with the experimental reports; the practically computed variables demonstrate the relevance to the existing research.

The outer region is regarded as being comprised of muffin-tin (MT) spheres, by which radial options are utilized, and the interstitial area is considered as the exact place where plane wave basis set is used. The particular core states are usually computed fully-relativistically and the valence states are computed scalar-relativistically. The MT radii of Ca, Sr, Ge as well as O are considered to be 2.53 a.u. (a.u. means atomic units), 2.14 a.u., 2.23 a.u., and 2.41 a.u, respectively. To obtain the ground state properties, we modify the first set of guidelines as $R_{\mathrm{MT}} \times K_{\max} = 8$ exactly, where R_{MT} is referred to as the Muffin-tin radius and $K_{\max}$ is known as the maximal value of the plane wave cutoff in the reciprocal plane and the angular momentum vector is held at $l_{\max} = 10$. To achieve the finest convergence, the group of k-points selected by means of script method and also k-mesh is generated for 1000 k-points on the order of $20 \times 20 \times 20$. The Gaussian parameter is selected as $G_{\max} = 12$. The energy is focalized up to $< 10^{-4}$ Ry. Finally, the structures enhanced by TB-mBJ are usually used to compute the thermoelectric properties of the studied materials through using the BoltzTrap code.

3. Results and discussion

3.1. Mechanical behavior

The relaxed constructions of $AGeO_3$ (A = Ca, Sr) perovskites are usually optimized into cubic phase to be able to compute the ground state variables through the use of PBEsol estimations. The computed ground state energy is

fitted directly into Murnaghan expression[28] for minimalvolume. The extracted estimations of lattice constant a(Å), modulus B (GPa) and its pressure derivative, and other quantities are given in Table 1. It really is apparent from Table 1 that the value regarding lattice continual a (Å) rises for $SrGeO_3$ as compared with that for $CaGeO_3$, although modulus B (GPa) lowers as the atomic dimension of cation increases from Ca to Sr, in which the inter-atomic length is raised. To affirm the mechanical stability, the entire arrangement of elastic properties is explored and displayed in Table 1. The elastic properties give the information about the capacity of a material to endure stress.[29] We have utilized Charpin technique, which is executed in Wien2K code,[25] to compute the elastic constants for $AGeO_3$ (A = Ca, Sr) and has been used in Refs. [30]–[32]. The particular cubic symmetry requires simply a three self-sufficient elastic constants C_{11}, C_{12}, and C_{44} to analyze the compound mechanical properties. On the other hand, three equations are needed to estimate these constants.[33] Based on the Born criterion of mechanical stability within a cubic framework,[34] the conditions $C_{11}-C_{12}>0$, $C_{44}>0$, $C_{11}+2C_{12}>0$, and $C_{12}<B_0<C_{11}$ are confirmed for the studied materials. The bulk modulus computed with elastic constants through the expression $B=(1/3)\ (C_{11}+2C_{12})$, which provides the values almost like the bulk modulus acquired through structural optimization which verifies the precisions in our outcomes (Table 1).

Table 1. Values of lattice parameter a (Å), Bulk modulus B (GPa), tndirect bandgap E_g (eV), elastic constant C_{ij} (GPa), Kleinman parameter (ζ), anisotropy factor (A), shear modulus G (GPa), Young's modulus E (GPa), Poisson's ratio ν, B/G ratio, Debye temperature (Θ_D), static $\varepsilon_1(0)$, $n(0)$ and $R(0)$ at equilibrium for $CaGeO_3$ and $SrGeO_3$ compounds calculated by using FP-LAPW-GGA (PBE).

Parameter	$CaGeO_3$	$SrGeO_3$
a/Å	3.742	3.807
B/GPa	193.14[a], 191.24[b]	180.31[a], 178.25[b]
E_g/eV	2.946	2.258
C_{11}/GPa	354.10	305.39
C_{12}/GPa	109.82	114.68
C_{44}/GPa	153.46	145.99
ζ	0.456	0.516
A	1.256	1.531
G/GPa	140.06	123.07
E/GPa	337.73	300.14
ν	0.205	0.219
B/G	1.365	1.448
Θ_D	19.07	15.87
$\varepsilon_1(0)$	3.188	3.376
$n(0)$	1.785	1.837
$R(0)$	0.0795	0.087

[a]From Murnaghan equation of state Ref. [28].

[b]From $B=(C_{11}+2C_{12})/3$.

Kleinman parameter (ζ) specifies bonding dynamics regarding material. The zero value contributes to bond folding and also corresponds to the bond stretching behavior. For that reason, each of our computations favors the particular bond stretching (see Table 1) in comparison with bond bending dynamics.[35] The elastic anisotropy is an additional essential parameter which is an indicator concerning the mini splits in the manufactured materials.[36] The elastic moduli (B, G, E) acquired from a couple of well-known approximations in Refs. [37]–[39] reduces the values of (B, G, E) from Ca to Sr. Furthermore, the computed value of Poisson's percentage (ν) is related to bulk modulus (B) and shear modulus (G) through the equations in Refs. [40] and [41], which are shown in Table 1. The Poisson's proportion describes the bonding forces inside the compounds. The top and bottom essential limits with the Poisson's proportion values which identifies the main forces inside materials are usually 0.25 to 0.50.

Consequently, it may be observed from Table 1 that how the forces acting on the materials tend to be central.[42] The elastic anisotropy could be predicted from the formula $A=2C_{44}/(C_{11}-C_{12})$ and it is displayed in Table 1. It is indeed 1 for isotropic materials and the value drops through 1 for these types of materials with anisotropic structures.[43] Additionally, it is clearly visible from Table 1 that $SrGeO_3$ can be more anisotropic than $CaGeO_3$. The particular structural stabilities are investigated with respect to Poisson ratio (υ) and Pough's proportion (B/G). In the conventional case, the ductile behavior can be discriminated from the brittle behavior for the considered materials,the Poisson ratio (υ) and Pough's proportion (B/G) tend to be 1.75 and 0.26 these values are below their limits at which the materials tend to be brittle ductile.It is really apparent from the Table 1, the examined materials are brittle and its behavior turns to be less brittle after $CaGeO_3$ has been converted into $SrGeO_3$. Finally, the Debye temperature is figured through the expression in Ref. [44], and listed in the Table 1. The estimation of Debye temperature is high for $CaGeO_3$ than for $SrGeO_3$.

3.2. Electronic properties

The electronic properties of these compounds could be exposed through their band structures. From the band structures (demonstrated in Fig. 2) of $CaGeO_3$ and $SrGeO_3$, it is seen that the highest points of the valence bands (VBs) are situated at M symmetric points, while the bases of the conduction bands (CB) are at Γ symmetric point. Subsequently, both the compounds possess indirect bandgap (Γ–M) natures. The bandgap for cubic $CaGeO_3$ is 2.95 eV and that for $SrGeO_3$ is 2.26 eV. As for our finest information, there are absolutely no fresh experimental outcomes or even additional theoretical estimations of the bandgaps of the perovskite materials that can be compared with our results. However, as a result of use of large k-points inside the irreducible Brillion zones (IBZ) and

by employing the state-of-the-artBecke Johnson (mBJ) potential, we are confident of the accuracy and reliability of the final results.

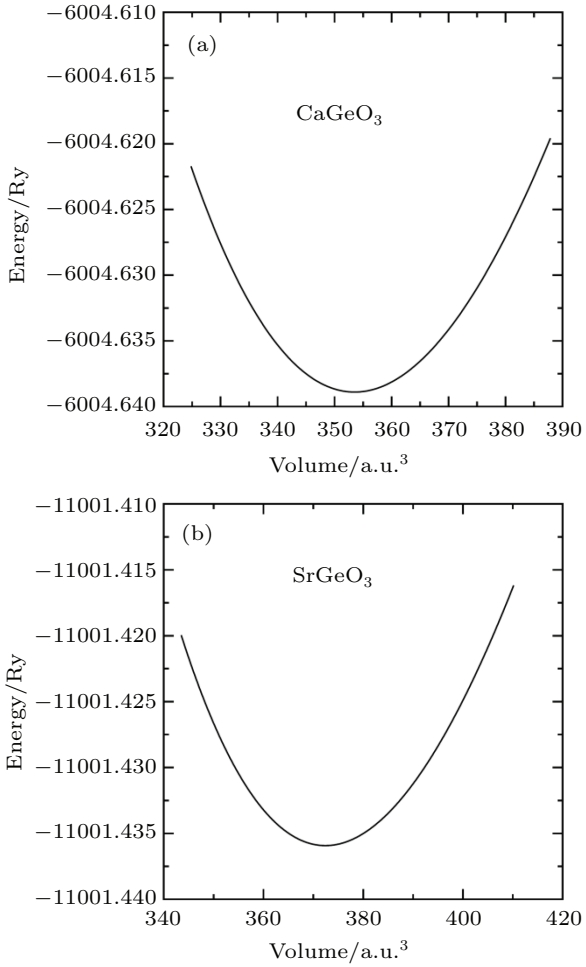


Fig. 1. Volume optimization plots of $CaGeO_3$ (a) and $SrGeO_3$ (b) by using the PBEsol approximation.

The information about the electron density of states (DOS) is needed to comprehend and clarify the band structures, bonding character, dielectric function, etc. of a compound. To understand these kinds of properties, we now determine the total densities of states (TDOSs) associated with these compounds. The projected DOSs for $CaGeO_3$ and $SrGeO_3$ may also be computed, which can be utilized to scrutinize the orbitals of diverse states. The TDOSs and partial densities of states (PDOSs) of the studied materials are usually plotted in Fig. 3. We could divided aparticular TDOS of the mentioned compounds directly into a few regions. The very first region is in a range from −8 eV to −4 eV is principal, because of the Ge-4p condition. The second area is in a range from −4 eV to 0 eV and is actually VB that includes O-2p state with a small factor coming from the Ca/Sr-4s/5s state. While, over the Fermi level, the band is CB composed of various states with small factors coming from Ge-4p, O-2p, and Ca/Sr-4s/5s that is visible.

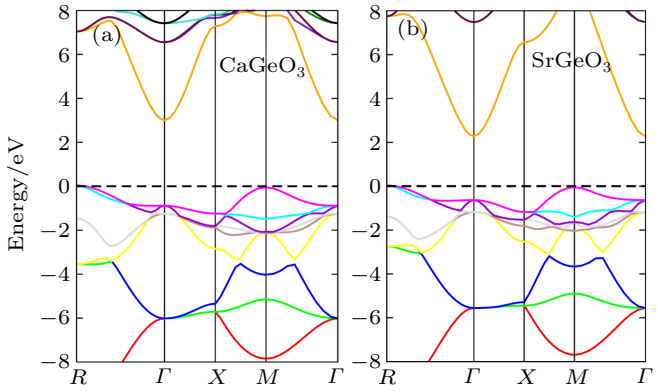


Fig. 2. (color online) Plots of calculated electronic band structures of $CaGeO_3$ (a) and $SrGeO_3$ (b) by using the mBJ potential.

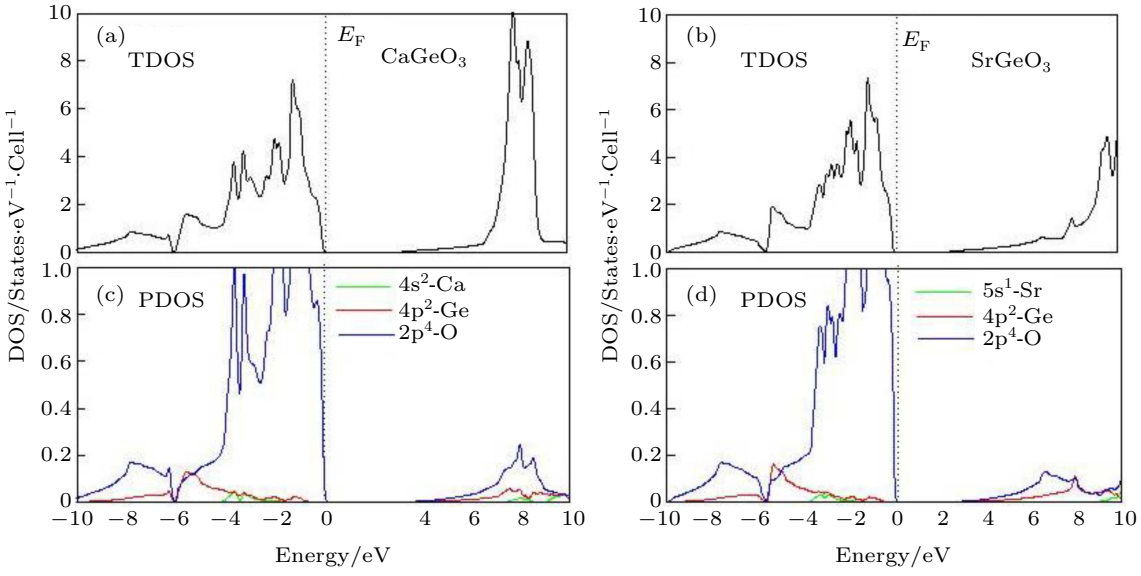


Fig. 3. (color online) Plots of TDOSs ((a) and (b)) and PDOSs ((c) and (d)) of $CaGeO_3$ and $SrGeO_3$ by using the mBJ potential.

3.3. Optical properties

As a way to elucidate this particular structures reviewed in the optical spectra, it is vital to straightly count transitions from occupied to unoccupied states, specifically with high symmetric points inside the Brillion zoon. The optical behavior of the physical arrangement within the sight of external electromagnetic radiations is described by the dielectric function $\varepsilon(\omega) = \varepsilon_1(\omega) + \varepsilon_2(\omega)$. The momentum matrix components are employed to ascertain the imaginary part, $\varepsilon_2(\omega)$, by following the selection rules for the optical transitions between the occupied and unoccupied states. The real part $\varepsilon_1(\omega)$ can be obtained from $\varepsilon_2(\omega)$ by applying Kramer–Kronig expression.[45] This imaginary part of dielectric function is expressed by

$$\varepsilon_2(\omega) = \frac{e^2 h'}{\pi m^2 \omega^2} \sum_{v,c} \int_{\mathrm{BZ}} |M_{cv}(k)|^2 \, \delta[\omega_{cv}(k) - \omega] \, \mathrm{d}^3 k, \quad (1)$$

in which the dipole matrix element $M_{cv}(k) = \langle u_{ck} | e\nabla | u_{vk} \rangle$ provides us with the details about transitions through conduction band to valence band. The real part of dielectric function is acquired from the Kramers–Kronig expression as follows:[45]

$$\varepsilon_1(\omega) = 1 + \frac{2}{\pi} P \int_0^{\infty} \frac{\omega' \varepsilon_2(\omega')}{\omega'^2 - \omega^2} \, \mathrm{d}\omega'. \quad (2)$$

The calculated optical parameters of $A\mathrm{GeO_3}$ (A = Ca, Sr) in an energy range of 20 eV are displayed in Figs. 4(a)–4(d) and 5(a)–5(d). It is really well worth revealing that despite the fact that TB-mBJ potential gives approximately precise Kohn–Sham eigenvalues, optical properties computed utilizing DFT estimations for an extensive variety of incident photon energy may not totally coincide with experimental results. A noteworthy reason for this contradiction is because of the interaction of energized electrons with holes (excitons). This involves the calculation relating to dielectric function using the additional electron–hole interaction (excitonic result) which can be an extremely difficult method and also usually not incorporated directly into DFT codes.

We compute the value of $\varepsilon_2(\omega)$ and plotted it in Fig. 4(b). At zero pressure the threshold values are 2.90 eV and 2.25 eV for $\mathrm{CaGeO_3}$ and $\mathrm{SrGeO_3}$ respectively, which relate to the optical bandgaps of the considered materials. Right after that, the values of $\varepsilon_2(\omega)$ are greatly enhanced and reach to maximal values at 8 eV for $\mathrm{CaGeO_3}$ and at 9 eV for $\mathrm{SrGeO_3}$, after that the values decease at different rates associated with inter-band and intra-band transitions. The peak shifting to maximum energy for $\mathrm{SrGeO_3}$ clarifies that the material is red-shifted as moving through Ca to Sr. This discovered transferring of peak to maximum energy is especially confirmed to be the electronic transition from O-2p state of VB to Ca/Sr-3p/4p state in the CB.

The frequency dependent $\varepsilon_1(\omega)$ is shown in Fig. 4(a). It could be noticed from Table 1 and this figure that the zero frequency limit, $\varepsilon_1(0)$ and optical band gap of the examined materials tend to be in precise accordance with the results obtained from Penn's model $\varepsilon_1(0) \approx 1 + (\hbar\omega_p / E_{\mathrm{g}})^2$. The $\varepsilon_1(\omega)$

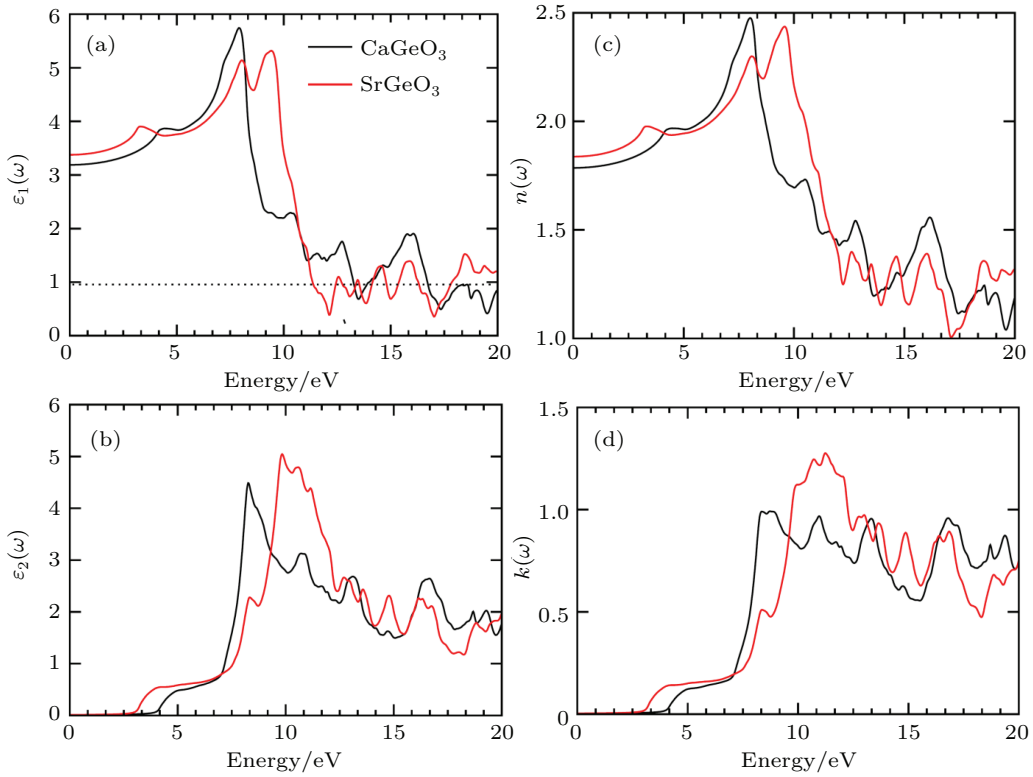


Fig. 4. (color online) Energy–dependent optical parameters: (a) real part of dielectric constant, (b) imaginary part of the dielectric constant, (c) refractive index, and (d) extinction coefficient for $\mathrm{CaGeO_3}$ and $\mathrm{SrGeO_3}$ by using the mBJ potential.

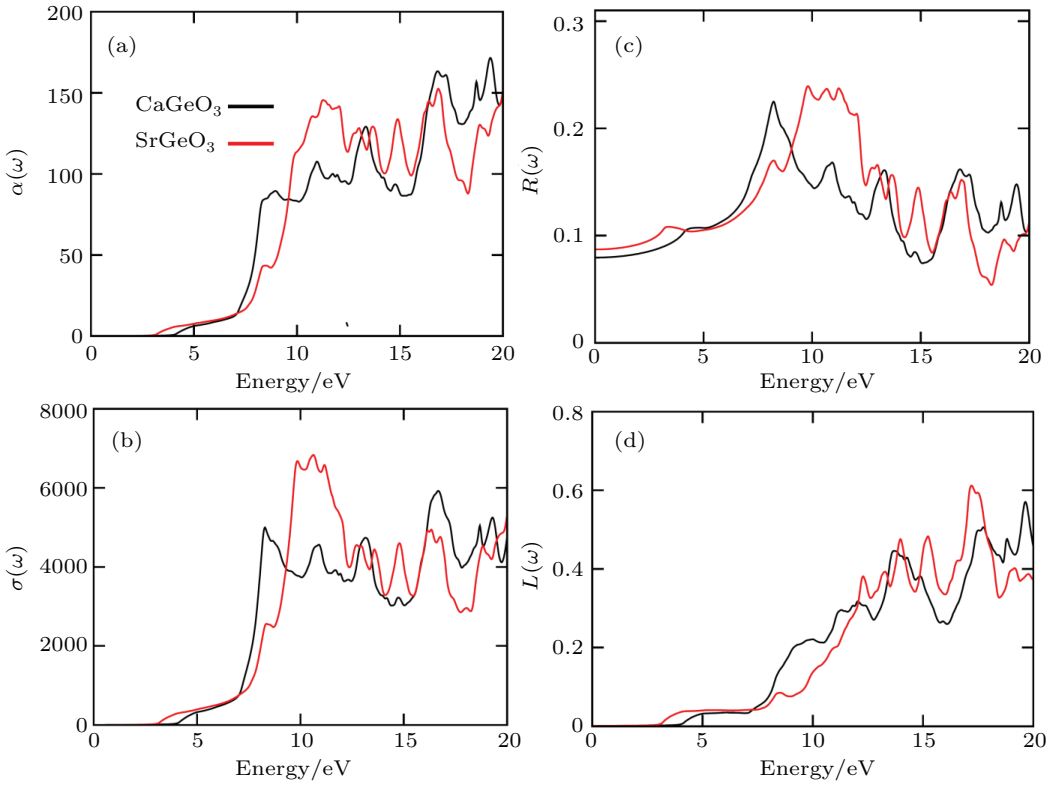


Fig. 5. (color online) Energy–optical parameters: (a) absorption coefficient, (b) optical conductivity, (c) reflectivity, and (d) optical loss factor for $CaGeO_3$ and $SrGeO_3$ by using the mBJ potential.

presents the information about the polarization from the compound, in which the measures are optimal from 7 eV for $CaGeO_3$ and from 9 eV for $SrGeO_3$, respectively. After that, the $\varepsilon_1(\omega)$ values often decrease to bare minimal values monotonically when frequency a bit changes due to resonance. These multitudes of modest peaks from the excessive energy could be due to diverse rates of electronic transitions.[46]

The refraction and dielectric constant possess balance correspondence; mean refractive index $n(\omega)$ and extinction coefficients $k(\omega)$ may be the reproduction of the real and imaginary which are demonstrated in Figs. 4(c) and 4(d). Thus, $n(\omega)$ and $k(\omega)$ are related through the mathematical expressions $n^2 - k^2 = \varepsilon_1(\omega)$ and $2nk = \varepsilon_2$. The $n(\omega)$ provides a measure of the transparency rate of the analyzed material that has adirect connection using the polarization described within Figs. 4(a) and 4(c) while $k(\omega)$ shows the absorption of light comparable to $\varepsilon_2(\omega)$. An additional essential point is the static measure associated with $n(\omega)$ and real part of the dielectric constant $\varepsilon_1(\omega)$ which satisfies the equation $n_0^2 = \varepsilon_1(0)$ and is demonstrated in Table 1.

The absorption coefficient $\alpha(\omega)$ and extinction coefficients $k(\omega)$ are usually related by the expression $\alpha = 4\pi k/\lambda$, which displays not only absorption coefficient $\alpha(\omega)$, but also extinction coefficients $k(\omega)$ and holds the identical behavior for the wave length of light. The absorption begins from a critical value referred to as optical bandgap and increases to a most extreme value with peak intensity increasing because of diverse rate of transition as clarified previously. Furthermore, it is obvious in Fig. 5(b) that the behavior associated with optical conductivity plot is nearly comparable to the absorption coefficient simply because of the enhancement of striking energy of electromagnetic radiation from the optical band gap of the compounds, the surplus energy is consumed through the electrons, there by enhancing their own kinetic energy to create the forward current within the apparatus.

The one additional imperative and essential parameter is the reflectivity that is revealed from the surface morphology of the compounds is shown in Fig. 5(c). The reflectivity is enhanced inside an area exactly where absorption along with optical conductivity diminishes on the grounds that at high energy (more than band gap), three sources of action (absorption, conductivity along with reflection) occur concurrently, which is revealed from the expression $(\alpha + T + R = 1)$. Finally, this optical loss functionality express the loss of energy through heat scattering and is usually minimal in the visible region and begins to improve in the infrared region, leading to excessive energy. Consequently, the entire evaluation through the optical properties from the studied material exhibits that within the visible region and the region close to infrared region, the absorption is actually optimal with minimal polarization, reflectivity as well as optical loss factor. This verifies the suitability of the studied materials intended to the manufacturing of optoelectronic devices.

3.4. Thermoelectric properties

Using DFT information and Boltzmann transportation theory (BTT),[24,25] the thermoelectric properties of these types of $AGeO_3$ (A = Ca, Sr) aredetermined. The BOLTZTRAP code is utilized to implement these calculations. The thermoelectric properties are primarily identified with the curvature of bands.[26] The real estimation of bandgap does not have a substantial influence on the thermoelectric property, even though the band gaps of semiconductors are usually underestimated in DFT computations as a result of neglecting them any-electron interactions. The BTT can still be used to efficiently measure the thermo–electric properties. The growing requirement and less amount of available electricity production make the thermoelectric material a prospective contender for the sustainable energy appliances. Most of the obtainable energy is lost as heat energy during power production and depleting of appliances. This lost energy of this kind may be restored from the skillful thermoelectric appliances.

As outlined in this article, the particular thermoelectric attributes associated with $AGeO_3$ (A = Ca, Sr) perovskites can be tackled when the electric conductivity (σ/τ), thermal conductivity, Seebeck coefficient, power factor and as well as thermoelectric effectiveness are obtained. The measured plot of electric conductivity (σ/τ) for $AGeO_3$ at temperatures in a range from 0 K to 800 K is displayed with Fig. 6(a). This electrical conductivity plot demonstrates that at 0 K, studied materials possess minimal electric conductivities 0.2×10^{19} ($\Omega^{-1}\cdot m^{-1}\cdot s^{-1}$) for $SrGeO_3$ and 0.6×10^{19} ($\Omega^{-1}\cdot m^{-1}\cdot s^{-1}$) for $CaGeO_3$, respectively. With temperature increasing to 800 K, the electrical conductivities reach to a 2.5×10^{19} ($\Omega^{-1}\cdot m^{-1}\cdot s^{-1}$) for $SrGeO_3$ and 2.6×10^{19} ($\Omega^{-1}\cdot m^{-1}\cdot s^{-1}$) for $CaGeO_3$, respectively. Heat conductions in the compounds generally take place because of the existence of electrons and phonons (lattice vibrations).

Thermal conductivities ((κ/τ) ($W\cdot m^{-1}\cdot K^{-1}\cdot s^{-1}$)) computed for the studied materials are demonstrated in Fig. 6(b), which increase greatly as the temperature rises. Thermal conductivities of the materials reach maximal values at 800 K. Thermoelectricity is actually produced whenever a couple of distinct components is usually placed in different temperature ranges. This kind of temperature gradient generates a specific voltage behavior between these two components. For any provided temperature gradient, a greater value of thermoelectric voltage leads to a greater effectiveness. The particular Seebeck coefficient (S) decides the efficiency of the thermocouple and it is also corresponding to the rate of the voltage variation towards the temperature fluctuation. The measured values associated with S values of the materials are shown in Fig. 6(c). The overall Seebeck coefficients for the materials rises until temperature rises up to 400 K, after that, with temperature rising to 800 K, the values of S are almost unchanged.

The power factor possesses a significant usage in estimating the overall functionality of the thermoelectric supply.[47]

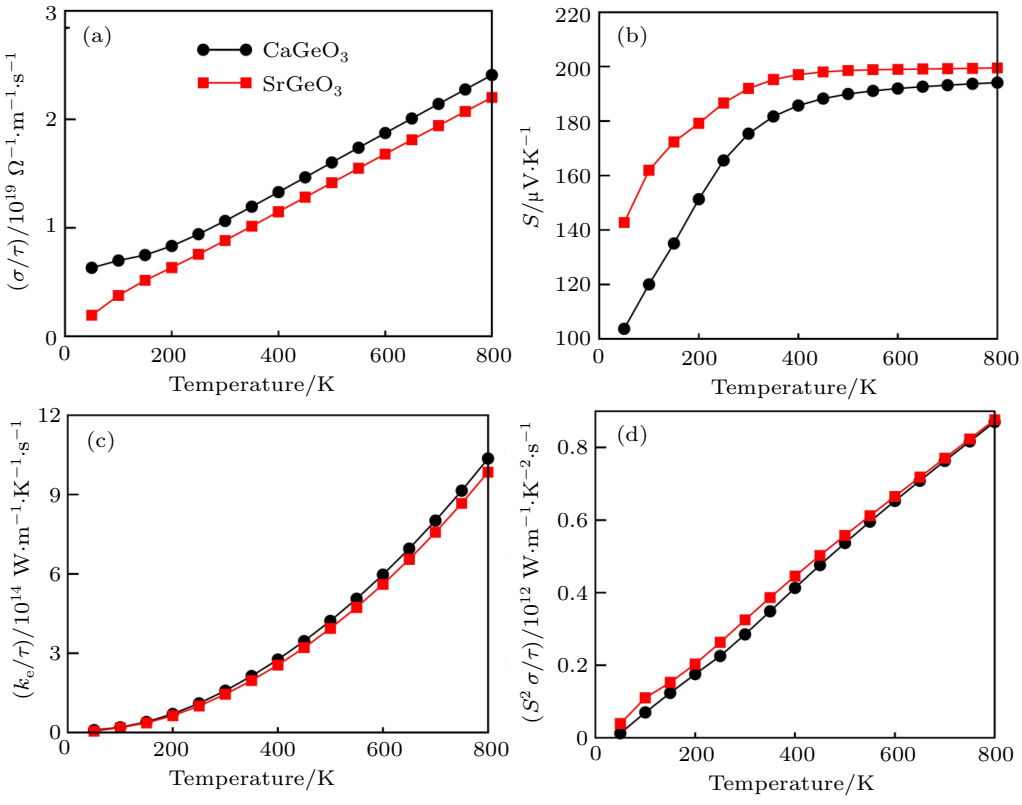


Fig. 6. (color online) Temperature-dependentthermoelectric properties: (a) electrical conductivity, (b) thermal conductivity, (c) Seebeck coefficient, and (d) power factor for $CaGeO_3$ and $SrGeO_3$ by using the BolTztraP code.

The power is specifically relevant to this electrical conductivity and the Seebeck coefficient and contains inverse relationship with the thermal conductivity. The determined values associated with power function versus temperature are demonstrated in Fig. 6(d). The power factor value rises with temperature increasing.

4. Conclusions

The mechanical, optical, and thermoelectric behaviors of the $AGeO_3$ (A = Ca, Sr) perovskite materials are investigated systematically in this paper. The bulk moduli decrease despite the fact that lattice parameter is raised from $CaGeO_3$ to $SrGeO_3$. Through elastic constants, it is discovered that the analyzed compounds possess ductile characters. Furthermore, the computations of band structures and the density of states of these studied compounds demonstrate the indirect bandgap (Γ–M) characters and the decrease in band gap from $CaGeO_3$ to $SrGeO_3$ in the visible range of electromagnetic spectrum. The zero frequency limits of $\varepsilon_1(\omega)$, $n(\omega)$, and $R(\omega)$ differ from the results obtained using the bandgaps associated with each studied material. In addition, the absorption is optimal in the region exactly where polarization is minimal. Moreover, the absorption coefficient and optical conductivity reach highest values in the ultraviolet region through which reflectivity and energy loss functions are lowest. The electric conductivity and Seebeck coefficient integrate in a way that the power factor is improved as the growing pattern associated with thermal conductivity is quite gradual. Consequently, thermal efficiencies in the analyzed materials are definitely higher. In addition to this, the assessments of the studied materials show that $CaGeO_3$ is a more effective compound for thermoelectric applications than $SrGeO_3$.

References

[1] Sarma D, Shanthi N, Barman S, Hamada N, Sawada H and Terakura K 1995 *Phys. Rev. Lett.* **75** 1126
[2] Kim J Y and Grishin A M 2006 *Thin Solid Films* **515** 2615
[3] Hao L J, Zhang D and Feng S H 2012 *Feng Funct. Mater.* **10** 43
[4] Zhong W, Chak-Tong A and Du Y W 2013 *Chin. Phys. B* **22** 057501
[5] Zhu X H, Zhang T, Cheng Y, Chen X R and Cai L C 2013 *Physica B: Condens. Matter* **411** 81
[6] Liu L G and Ringwood A 1975 *Earth Planet. Sci. Lett.* **28** 209
[7] Liebermann R C 1976 *Earth Planet. Sci. Lett.* **29** 326
[8] Sasaki S, Prewitt C T, Bass J D and Schulze W 1987 *Acta Crystallogr C* **43** 1668
[9] Tanaka M, Shishido T, Horiuchi H, Toyota N, Shindo D and Fukuda T 1993 *J. Alloys Compd.* **192** 87
[10] Zerr A, Diegeler A and Boehler R 1998 *Science* **281** 243
[11] Sasaki S, Prewitt C T and Liebermann R C 1983 *Am. Mineral.* **68** 1189
[12] Redfern S A 1996 *J. Phys.: Condens. Matter* **8** 8267
[13] Liu X, Wang Y, Liebermann R, Maniar P and Navrotsky A 1991 *Phys. Chem. Miner.* **18** 224
[14] Durben D J, Wolf G H and McMillan P F 1991 *Phys. Chem. Miner.* **18** 215
[15] Andrault D and Poirier J 1991 *Phys. Chem. Miner.* **18** 91
[16] Lu R and Hofmeister A M 1994 *Phys. Chem. Miner.* **21** 78
[17] Liu W and Li B 2007 *Phys. Rev. B* **75** 024107
[18] Grzechnik A, Hubert H, McMillan P and Petuskey W 1997 *Integr. Ferroelectr.* **15** 191
[19] Yamaguchi O, Sasaki H, Sugiura K and Shimizu K 1983 *Ceram. Int.* **9** 75
[20] Fang C M and Ahuja R 2006 *Phys. Earth Planet. Inter.* **57** 1
[21] Henriques J, Caetano E, Freire V, da Costa J and Albuquerque E L 2007 *J. Solid State Chem.* **180** 974
[22] Gudelli V K, Kanchana V, Appalakondaiah S, Vaitheeswaran G and Valsakumar M 2013 *J. Phys. Chem. C* **117** 21120
[23] Lu X and Morelli D T 2013 *Phys. Chem. Chem. Phys.* **15** 5762
[24] Madsen G K, Singh D J and BoltzTra P 2006 *Comput. Phys. Commun.* **175** 67
[25] Blaha P, Schwarz K, Madsen G, Kvasnicka D and Luitz J 2001 *WIEN2k: An Augmented Plane Wave Plus Local Orbitals Program for Calculating Crystal Properties*
[26] Perdew J P, Ruzsinszky A, Csonka G I, Vydrov O A, Scuseria G E, Constantin L A, Zhou X and Burke K 2008 *Phys. Rev. Lett.* **100** 136406
[27] Becke A D and Johnson E R 2006 *J. Chem. Phys.* **124** 221101
[28] Murnaghan F 1944 *Proc. Natl. Acad. Sci.* **30** 244
[29] Reshak A H and Jamal M 2012 *J. Alloys Compd.* **543** 147
[30] Hassan F E H and Akbarzadeh H 2006 *Comput. Mater. Sci.* **38** 362
[31] Khenata R, Bouhemadou A, Sahnoun M, Reshak A H, Baltache H and Rabah M 2006 *Comput. Mater. Sci.* **38** 29
[32] Bouhemadou A, Khenata R, Kharoubi M, Seddik T, Reshak A H and Al-Douri Y 2009 *Comput. Mater. Sci.* **45** 474
[33] Monir M E A, Baltache H, Khenata R, Murtaza G, Azam S, Bouhemadou A, Al-Douri Y, Omran S B and Ali R 2015 *J. Magn. Magn. Mater.* **378** 41
[34] Nye J F 1985 *Physical Properties of Crystals: Their Representation by Tensors and Matrices* (Oxford: Oxford University Press)
[35] Jamal M, Asadabadi S J, Ahmad I and Aliabad H R 2014 *Comput. Mater. Sci.* **95** 592
[36] Tvergaard V and Hutchinson J W 1988 *J. Am. Ceram. Soc.* **71** 157
[37] Hill R 1952 *Proc. Phys. Soc. London* **65** 349
[38] Voigt W 1910 *Lehrbuch der Kristall Physik Teubner* (Leipzig) *(reprinted (*1928*) with an additional Appendix)* (New York: Johnson Reprint)
[39] Reuss A 1929 *J. Appl. Math. Mech.* **9** 49
[40] Wu Z J, Zhao E J, Xiang H P, Hao X F, Liu X J and Meng J 2007 *Phys. Rev. B* **76** 054115
[41] Peng F, Chen D, Fu H and Cheng X 2009 *Phys. Status Solidi* **246** 71
[42] Fu H, Li D, Peng F, Gao T and Cheng X 2008 *Comput. Mater. Sci.* **44** 774
[43] Zhang W B, Zeng F and Tang B Y 2015 *Chin. Phys. B* **24** 097103
[44] Anderson O L 1963 *J. Phys. Chem. Solids* **24** 909
[45] Marius G 2010 *Kramers–Kronig Relations* in *The Physics of Semiconductors* (Berlin, Heidelberg: Springer) pp. 775–776
[46] Wang S, Du Y L and Liao W H 2017 *Chin. Phys. B* **26** 017806
[47] Kulwinder K and Ranjan K 2016 *Chin. Phys. B* **25** 026402